# Light-dependent regulation of structural flexibility in a photochromic fluorescent protein

Hideaki Mizuno*, Tapas Kumar Mal†, Markus Wälchli‡, Akihiro Kikuchi§, Takashi Fukano*, Ryoko Ando*, Jeyaraman Jeyakanthan§, Junichiro Taka§, Yoshitsugu Shiro§, Mitsuhiko Ikura†, and Atsushi Miyawaki*¶

*Cell Function and Dynamics, Brain Science Institute, RIKEN, 2-1 Hirosawa, Wako-City, Saitama 351-0198, Japan; †Division of Signaling Biology, Ontario Cancer Institute and Department of Medical Biophysics, University of Toronto, MaRS Toronto Medical Dicovery Tower, Room 4-804, 101 College Street, Toronto, ON, Canada M5G 1L7; ‡Bruker BioSpin K. K., 3-21-5, Ninomiya, Tukuba-City, Ibaraki 305-0051, Japan; and §Biometal Science Laboratory, RIKEN SPring-8 Center, 1-1-1 Kouto, Sayo-Cho, Sayo-Gun, Hyogo 679-5198, Japan

Edited by Roger Y. Tsien, University of California at San Diego, La Jolla, CA, and approved April 15, 2008 (received for review October 9, 2007)

**The structural basis for the photochromism in the fluorescent protein Dronpa is poorly understood, because the crystal structures of the bright state of the protein did not provide an answer to the mechanism of the photochromism, and structural determination of the dark state has been elusive. We performed NMR analyses of Dronpa in solution at ambient temperatures to find structural flexibility of the protein in the dark state. Light-induced changes in interactions between the chromophore and β-barrel are responsible for switching between the two states. In the bright state, the apex of the chromophore tethers to the barrel by a hydrogen bond, and an imidazole ring protruding from the barrel stabilizes the plane of the chromophore. These interactions are disrupted by strong illumination with blue light, and the chromophore, together with a part of the β-barrel, becomes flexible, leading to a nonradiative decay process.**

crystal structure | NMR | photochromism

Photochromism is defined as the reversible transformation of a single chemical species between two states having different absorption spectra induced by photoirradiation (1). Most of photochromic substances are organic compounds, including diarylethenes (2) and spiropyran (3). Dronpa is a photochromic fluorescent protein engineered from a coral protein (4). Whereas Dronpa normally absorbs at 503 nm and emits green fluorescence with a high fluorescence quantum yield ($\phi_{FL}$ = 0.85), strong irradiation at 488 nm can convert this protein to a nonfluorescent state that absorbs at 390 nm (dark state, denoted by Dronpa$^{D}$). The protein can then be switched back to the original emissive state (bright state, denoted by Dronpa$^{B}$) with minimal irradiation at 405 nm. Because of its reliable photochromic properties, Dronpa can be used to record, erase, or read information in a nondestructive manner (4).

Reversible transformation in photochromic systems has been studied in organic compounds (1). This process comprises hydrogen transfer, dimerization, cyclization, ring opening, and isomerization. It is unknown whether the photochromism exhibited by Dronpa employs similar mechanisms or a previously uncharacterized one that utilizes the unique structure of fluorescent proteins. Comparing the structures of Dronpa$^{B}$ and Dronpa$^{D}$ is essential to understand the mechanism of photochromism in Dronpa. Although three groups (5–7) have reported that the crystal structure of Dronpa$^{B}$ is similar to other fluorescent proteins, there is less structural information for Dronpa$^{D}$. Recently, *cis-trans* photoisomerization of the chromophore has been proposed as the structural basis of the Dronpa photochromism (8). However, *trans* configuration alone does not provide a photochemical explanation for nonfluorescence. In x-ray crystallographic studies, protein crystals are commonly frozen to 80 K to reduce radiation damage and thermal vibrations to lower conformational disorder and improve the quality of the model. However, in our initial crystallographic studies, we observed that our crystals of Dronpa were resistant to phototransformation at 80 K but not at room temperature (298 K). Thus, we used NMR analyses near room temperature to explore the dynamic structure of Dronpa$^{D}$ unattainable by crystallographic methods at 80 K.

## Results

**Photoresistance of Dronpa at Low Temperatures.** We also determined the Dronpa$^{B}$ crystal structure at 1.75-Å resolution; the overall and chromophore structures are shown in Fig. 1 *A* and *B*, respectively. In an attempt to determine the crystal structure of Dronpa$^{D}$, we performed photoirradiation experiments with these crystals using the 514.5-nm line of an argon ion laser. Interestingly, whereas the 514.5-nm light dimmed the crystals efficiently at 298 K, the crystals were resistant to transformation at 80 K on the x-ray beam line for crystallography [supporting information (SI) Fig. S1]. The photoresistance of Dronpa at low temperatures was also verified in solution with experiments by using the Joule–Thompson apparatus (R.A., H.M., and A.M., unpublished results).

**Flexibility Found in the β-Barrel of Dronpa$^{D}$.** To explore a possibly dynamic structure of Dronpa$^{D}$, we performed solution NMR analyses using both Dronpa$^{B}$ and Dronpa$^{D}$. The difficulty of these experiments was compounded by the fact that Dronpa$^{D}$ is not stable for days; Dronpa$^{D}$ converts to Dronpa$^{B}$ gradually even in the dark (4). During ≈3 days of NMR measurements, we maintained Dronpa$^{D}$ by continuous illumination at 514.5 nm by means of an optical fiber connected to a 150-mW argon ion laser. The protein sample that had experienced the long-term laser illumination displayed a full dark-to-bright conversion upon illumination at 390 nm (Fig. S2).

Dronpa was uniformly labeled with $^{13}C$ and $^{15}N$, and NMR spectra were acquired for assignment of $^{13}C^{\alpha}$, $^{13}C^{\beta}$, $^{15}N$, and $^{1}HN$ resonances of Dronpa$^{B}$ and subsequently of Dronpa$^{D}$ (Fig. S3). The backbone assignment identified 93% and 83% of the residues of Dronpa in the Dronpa$^{B}$ and Dronpa$^{D}$ spectra, respectively; all prolines and the chromophore Tyr and Gly were excluded from the calculation, because they have no protons on their backbone nitrogens. Twenty-five peaks assigned for Dronpa$^{B}$ were not assigned for Dronpa$^{D}$ because of extensive linewidth

Author contributions: H.M., T.K.M., M.W., Y.S., M.I., and A.M. designed research; H.M., T.K.M., M.W., A.K., T.F., and R.A. performed research; H.M., M.W., A.K., and T.F. contributed new reagents/analytic tools; H.M., T.K.M., M.W., A.K., J.J., and J.T. analyzed data; and H.M. and A.M. wrote the paper.

The authors declare no conflict of interest.

This article is a PNAS Direct Submission.

Data deposition: The coordinates for Dronpa and 22G structures have been deposited in the Protein Data Bank, www.pdb.org (PDB ID codes 2Z1O, 2Z6Y, and 2Z6Z for Dronpa and 2Z6X for 22G).

¶To whom correspondence should be addressed. E-mail: matsushi@brain.riken.jp.

This article contains supporting information online at www.pnas.org/cgi/content/full/0709599105/DCSupplemental.

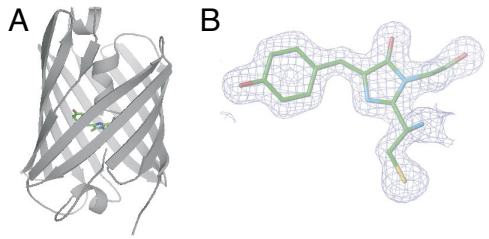


**Fig. 1.** Crystal structure of Dronpa$^{B}$ (PDB ID 2Z1O). (*A*) Overall structure is shown in the cartoon with the chromophore (stick format). (*B*) A $2F_o$-$F_c$ electron density map of the chromophore contoured at 1.2$\sigma$. A space group of the crystal was $P2_12_12_1$. We also solved structures of Dronpa$^{B}$ with space groups of $P2_1$ and $P2_12_12$ and obtained substantially the same results (PDB IDs 2Z6Y and 2Z6Z).

broadening. Conversely, one peak assigned for Dronpa$^{D}$ is missing in the Dronpa$^{B}$. The residues corresponding to the Dronpa$^{B}$- and Dronpa$^{D}$-specific peaks are positioned as magenta and blue bars, respectively, in the chemical shift difference (CSD) plot (9) (Fig. 2*A*). Seven residues show highly different chemical shifts between the Dronpa$^{B}$ and Dronpa$^{D}$ spectra. These residues are numbered in orange in the CSD plot (Fig. 2*A*). Most of the residues associated with these differential peaks are located on the $\beta$-strands near the chromophore hydroxyphenyl moiety, as painted in magenta, blue, and orange on the crystal structure of Dronpa$^{B}$ (Fig. 2 *B* and *C*). It was speculated that these colored regions in Dronpa$^{D}$ had a deviated structure from the Dronpa$^{B}$ $\beta$-barrel. In particular, the magenta region comprises 25 aa that were not assignable in Dronpa$^{D}$. We conclude that the magenta region in Dronpa$^{D}$ takes a polymorphic and flexible structure. This is consistent with the fact that we could not obtain the Dronpa dark state at 80 K, a temperature at which molecular motion is highly restricted (Fig. S1).

To characterize the Dronpa$^{D}$-specific structure of the $\beta$-strands, we analyzed histidine (His)-$^{13}C_6$,$^{15}N_3$-labeled Dronpa. Among the nine His residues in Dronpa, His-193, His-194, and His-212 reside in the differential regions. There were differences in the $^{1}H$-$^{15}N$ heteronuclear sequential quantum correlation (HSQC) spectra between Dronpa$^{B}$ and Dronpa$^{D}$ for only these three His residues (Fig. 2*D*). In the Dronpa$^{B}$ spectrum, each of the nine His residues was assigned as a sharp peak. In the Dronpa$^{D}$ spectrum, by contrast, the three sharp peaks corresponding to His-193, His-194, and His-212 were replaced by two broad peaks. This broadening of peaks is consistent with the greater flexibility of the $\beta$-strands containing H193, H194, and H212 in Dronpa$^{D}$.

**Chromophore Structures of Dronpa$^{B}$ and Dronpa$^{D}$.** Crystallographic models propose that Dronpa$^{B}$ has a rigid *cis*/coplanar chromophore (Fig. 1*B*). What structural changes near the chromophore would be associated with the structural flexibility we observe in the $\beta$-barrel of Dronpa$^{D}$? In most fluorescent proteins, the hydroxyphenyl moiety of a tyrosine residue within the chromophore-forming tripeptide is critical for fluorescence (10). This tyrosine is located at position 63 in Dronpa. To examine Tyr-63-related structures in Dronpa$^{B}$ and Dronpa$^{D}$, we labeled the protein with Tyr-$^{13}C_9$ and used a cryogenic TCI probe for direct detection of $^{13}C$ resonances at high sensitivity. A large downfield shift was observed for $C^{\zeta}$ of Tyr-63 to 177.0 ppm in the $^{13}C$-$^{13}C$ NOESY spectrum (11) for Dronpa$^{B}$ (Fig. 3*A*, magenta arrowhead). This indicates deprotonation of the hydroxyphenyl moiety as a rise in electron density by deprotonation increases electric shield. In contrast, no downfield shift was observed for $C^{\zeta}$ in the spectrum for Dronpa$^{D}$ (Fig. 3*A*). Therefore, we conclude that the hydroxyphenyl moiety is deprotonated in Dronpa$^{B}$ and protonated in Dronpa$^{D}$ (Fig. 3*C*, magenta arrowhead). The protonation/deprotonation equilibrium is consistent with NMR-based pH titration data (12, 13).

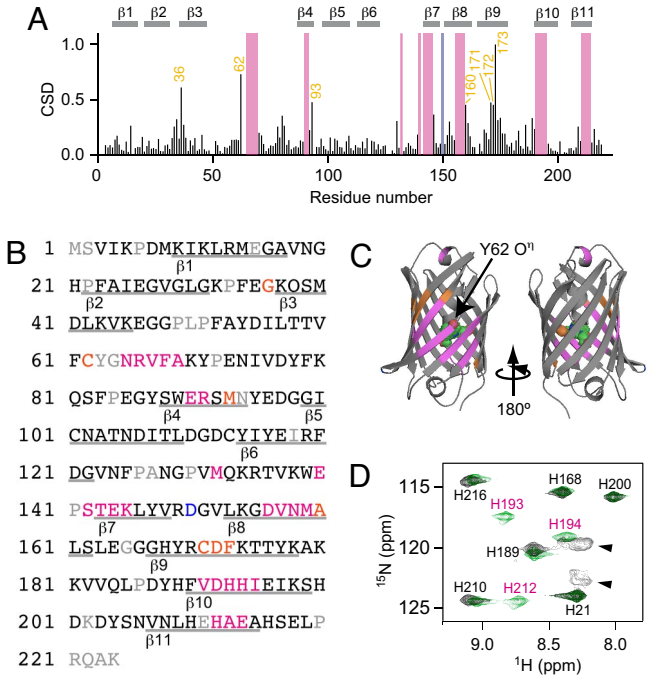


**Fig. 2.** $\beta$-Barrel structures of Dronpa$^{B}$ and Dronpa$^{D}$ analyzed by NMR spectroscopy. (*A*) Normalized weighted CSD between Dronpa$^{B}$ and Dronpa$^{D}$. CSD values >0.4 are marked with residue numbers in orange. Residues assigned specifically in Dronpa$^{B}$ and Dronpa$^{D}$ are highlighted with magenta and blue bars, respectively. (*B*) The Dronpa sequence in which the differential residues are indicated in the same color. (*C*) Mapping of the differential residues with magenta, blue, and orange on the Dronpa$^{B}$ crystal structure. (*D*) The $^{1}H$-$^{15}N$ HSQC spectra of His- $^{13}C_6$,$^{15}N_3$-labeled Dronpa$^{B}$ (green) and Dronpa$^{D}$ (black). Peaks are marked with amino acids (single letter code) and residue numbers. Dronpa$^{B}$-specific peaks are marked in magenta. Dronpa$^{D}$-specific broad peaks are indicated by arrowhead.

The $^{1}H$-$^{13}C$ HSQC spectra obtained from the Tyr-$^{13}C_9$-labeled Dronpa also provided important information about the conformation of the chromophore. In the spectrum for Dronpa$^{B}$, Tyr-63 $H^{\delta 2}$ displayed a substantial downfield shift that was apparently caused by a ring current effect of the imidazolinone ring (Fig. 3*B*, magenta arrow). This proton–ring interaction reveals the *cis* coplanar conformation of the chromophore (Fig. 3*C*, magenta arrow) also observed in the Dronpa$^{B}$ crystal structure (Fig. 1*A*). The downfield shift of Tyr-63 $H^{\delta 2}$ was never observed for Dronpa$^{D}$ (Fig. 3*B*), demonstrating that the $H^{\delta 2}$ is not on the same plane as the imidazolinone ring in the dark state.

**Light-Induced Regulation of Interaction Between the $\beta$-Barrel and Chromophore.** We propose that the hydroxyphenyl moiety of the chromophore and the $\beta$-strands near the moiety are fixed in Dronpa$^{B}$ but flexible in Dronpa$^{D}$. How is the rigidity and flexibility controlled? As the chromophore $O^{\eta}$ and the hydroxyl group of Ser-142 face each other in close proximity in the Dronpa$^{B}$ crystal (2.73 Å, Fig. 3*F*; see also Fig. S4), this interaction should be critical for tethering the chromophore to this $\beta$-barrel. In Dronpa$^{B}$, the deprotonated $O^{\eta}$ is negatively charged and forms a hydrogen bond with the Ser-142 hydroxyl hydrogen (Fig. S4). In contrast, in Dronpa$^{D}$, the protonated $O^{\eta}$ would not form this hydrogen bond. To determine whether this hydrogen bond exists exclusively in Dronpa$^{B}$, we examined $^{1}H$ NMR at −1.6°C because the proton resonance of a serine hydroxyl group can generally be detected at ≈14 ppm only when the group forms

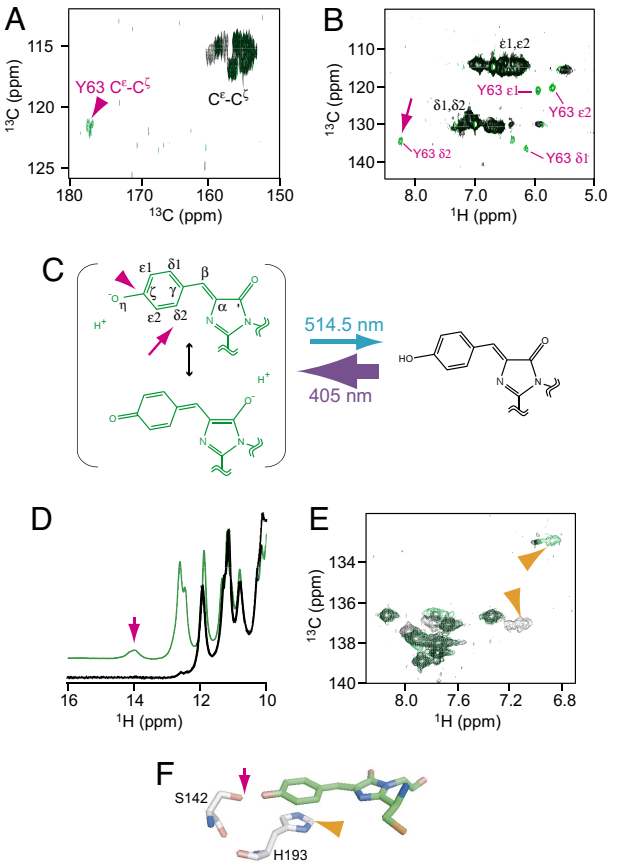


**Fig. 3.** Chromophore structures of Dronpa$^{B}$ and Dronpa$^{D}$ revealed by NMR analyses. (*A*) Expanded $^{13}C$-$^{13}C$ NOESY spectra of Tyr-$^{13}C_9$-labeled Dronpa$^{B}$ (green) and Dronpa$^{D}$ (black). Full $^{13}C$-$^{13}C$ NOESY spectrum of Tyr-$^{13}C_9$-labeled Dronpa$^{B}$ is shown in Fig. S5. A downfield shifted peak is assigned to Tyr-63 $C^{\varepsilon}$-$C^{\zeta}$ of Dronpa$^{B}$ (magenta arrowhead). (*B*) The $^{1}H$-$^{13}C$ HSQC spectra of Tyr-$^{13}C_9$-labeled Dronpa$^{B}$ (green) and Dronpa$^{D}$ (black). Peaks assigned for $C^{\delta1}$-$H^{\delta1}$, $C^{\delta2}$-$H^{\delta2}$, $C^{\varepsilon1}$-$H^{\varepsilon1}$, and $C^{\varepsilon2}$-$H^{\varepsilon2}$ of Dronpa$^{B}$ Tyr-63 are colored magenta. The $C^{\delta2}$-$H^{\delta2}$ correlation is evidenced by the downfield shift of the $^{1}H$ chemical shift (magenta arrow). (*C*) Light-dependent conversion between Dronpa$^{B}$ and Dronpa$^{D}$. Magenta arrowhead and arrow indicate $C^{\zeta}$ and $C^{\delta2}$-$H^{\delta2}$, respectively. (*D*) Expanded $^{1}H$ NMR spectra acquired at −1.6°C with U-$^{13}C$,$^{15}N$-labeled Dronpa$^{B}$ (green) and Dronpa$^{D}$ (black). Magenta arrow indicates a peak tentatively assignable to $^{1}H$ on hydroxyl group of Ser-142, which is detectable only in Dronpa$^{B}$. (*E*) Expanded $^{1}H$-$^{13}C$ HSQC spectra of His-$^{13}C_6$,$^{15}N_3$-labeled Dronpa$^{B}$ (green) and Dronpa$^{D}$ (black). Peaks tentatively assignable to $C^{\varepsilon1}$-$H^{\varepsilon1}$ of His-193 are indicated by orange arrowhead. (*F*) Relative position of the chromophore, Ser-142, and His-193. Hydroxyl group of Ser-142 (magenta arrow) and $C^{\varepsilon1}$ of His-193 (orange arrowhead) are indicated.

a hydrogen bond (14). A peak for the proton assigned to the Ser-142 hydroxyl group at 14.0 ppm was present only in the spectrum for Dronpa$^{B}$ (Fig. 3*D*). We confirmed the requirement of this hydrogen bond for the bright fluorescence of Dronpa by mutating this serine residue. Replacement of Ser-142 with Ala, Cys, Asp, or Gly generated Dronpa$^{D}$-like variants that absorbed light maximally at 390 nm (data not shown). Similar results were obtained by replacing Tyr-63 with Phe (data not shown).

As expected from the results of Fig. 2*D*, His-193, His-194, and His-212 may be in the flexible part of the β-strands in Dronpa$^{D}$. In the $^{1}H$-$^{13}C$ HSQC spectrum of His-$^{13}C_6$,$^{15}N_3$-labeled Dronpa, there was an upfield shift of His-193 $C^{\varepsilon1}$ in Dronpa$^{B}$ (Fig. 3*E*), consistent with a ring current effect of the chromophore phenyl moiety. Thus, the His-193 imidazole likely forms a stacking interaction with the chromophore in Dronpa$^{B}$ (Fig. 3*F*). Replacement of His-193 with Thr also prevented fixation of the chromophore and the resultant His193Thr mutant was nonfluorescent regardless of the protonation/deprotonation of the chromophore $O^{\eta}$ (data not shown).

**Quaternary Structure and Prevention of Conversion into Dronpa$^{D}$.** Substantial photochromism was originally identified in the course of mutagenesis studies that aimed at monomerizing 22G, a coral fluorescent protein that forms an obligate tetrameric complex. Like most other wild-type GFP-like proteins, 22G forms a tight tetrameric complex and shows no photochromism. Six mutations on 22G, namely, Ile102Asn, Phe114Tyr, Leu162Ser, Arg194His, Asn205Ser, and Gly218Glu on 22G have led to creation of the monomeric and photochromic fluorescent protein, Dronpa. It was thus hypothesized that the light-regulated structural flexibility observed in Dronpa was affected by oligomerization of the β-barrel structure.

The crystal structure of 22G was determined at 2.3-Å resolution (Fig. 4) and was compared with that of Dronpa$^{B}$. We notice two interesting features in the dimer complex between protomers A and C of 22G. First, the AC dimer interface is mostly composed of a pair of surface regions containing the flexible β-sheets characterized for Dronpa in this study. Second, the C termini of protomers A and C protrude into the interface to stabilize the flexible β-sheets of protomers C and A, respectively (Fig. 4 *A* and *B*). This unique C terminus-mediated interaction affects greatly the light-regulated structural flexibility. In fact, the replacement of Gly-218 with Glu conferred significant photochromic performance to 22G (Table 1). This mutation (Gly218Glu) appears to cause withdrawal of the C terminus, probably because of electrical repulsion between Glu-218 and Glu-140 (Fig. 4*B*). The C terminus-mediated interaction may not be necessary for the dimer formation; the Gly218Glu mutation on 22G preserved its tetrameric complex (Table 1). These results are consistent with the fact that the Dronpa$^{B}$ crystal data lack electron density information corresponding to the C terminus (Fig. 1).

In contrast, none of the flexible β-sheets was found at the AB dimer interface of 22G (Fig. 4 *A* and *C*). One of the critical amino acid residues for the dimer formation is Ile-102; two leucines on protomers A and B show hydrophobic interaction (Fig. 4*C*). The replacement of Ile-102 with Asn broke up the AB dimer interface partially, but did not induce conversion into the dark state (Table 1).

The 22G mutant carrying Gly218Glu and Ile102Asn is monomeric and photochromic, thus being comparable with Dronpa (Table 1). With the other four mutations initially introduced, 22G can be converted into Dronpa, which is truly monomeric and practically photochromic. Altogether, it is concluded that the flexibility of the surface region at the AC dimer interface is required to reach the dark state and that detachment of the C terminus from the flexible surface is essential to engineer photochromic fluorescent proteins from 22G.

## Discussion

We propose a structural basis for the bright and dark states of Dronpa (Fig. 5*A*). In the bright state, the chromophore is tethered to the β-barrel through the hydrogen bond between the chromophore hydroxyl oxygen and the Ser-142 hydroxyl group on the barrel wall. This hydrogen bond holds the two rings of the chromophore in a *cis* configuration. The His-193 imidazole ring is located below the chromophore phenyl moiety and stabilizes the entire chromophore in a coplanar conformation. This rigid structure favors the radiative relaxation process from the first electronic excited state ($S_1$) to the ground state ($S_0$). By contrast, in the dark state, the protonation of the chromophore hydroxyl moiety results in loss of both the hydrogen bond with Ser-142 and the chromophore stacking with His-193. These structural changes increase flexibility of not only the chromophore but also

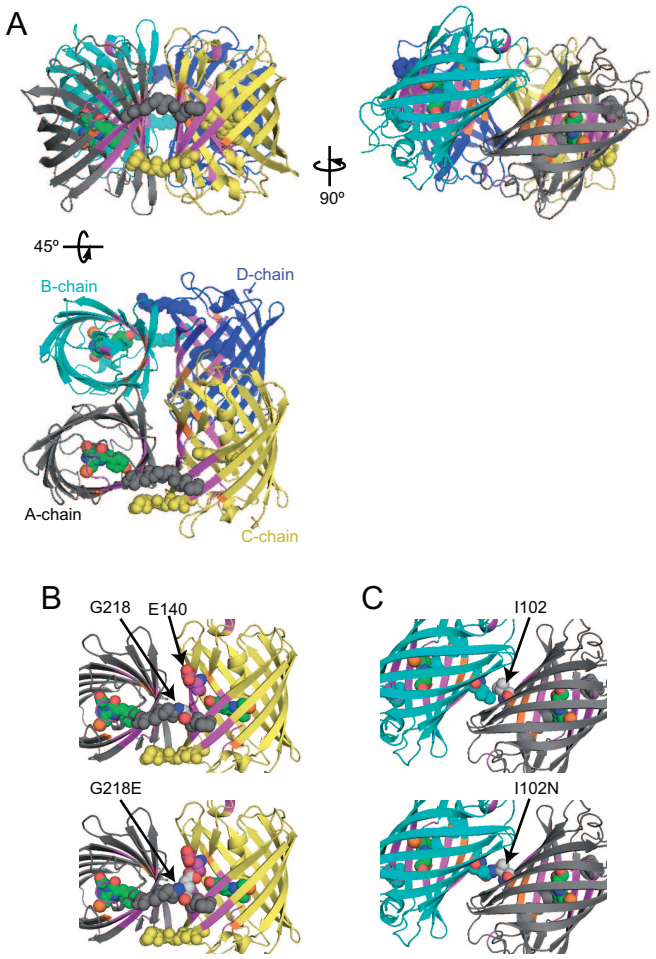


**Fig. 4.** Quaternary structure of 22G depicted in the cartoon with the chromophore (green, red, and blue spheres for carbon, oxygen, and nitrogen atoms) (PDB ID 2Z6X). Four protomers are depicted in different colors (gray, cyan, yellow, and blue for A, B, C, and D, respectively). The flexible surface regions are highlighted in magenta and orange as in Fig. 2. Main chains of the C-terminal regions are shown in spheres. (*A*) Tetrameric complex of 22G. Three views at different angles are shown. (*B* and *C*) AC–dimer interface (*B*) and AB–dimer interface (*C*) are zoomed in. (*Upper*) Solved crystal structures. (*Lower*) Modeled structures with substitutions of Gly218Glu (*B*) and Ile102Asn (*C*). Residues at 102 and 140 are depicted with spheres.

a part of the β-barrel (indicated in purple in Fig. 5*A*), favoring the nonradiative vibrational relaxation process. In a previous study, Seifert *et al.* (16) measured H–D exchange of a variant of *Aequorea* GFP, $GFP_{UV}$, by NMR and suggested a slightly flexible region on the β-barrel. In contrast, the flexibility we found in $Dronpa^{D}$ was remarkable because most of the resonance peaks corresponding to this region were undetectable.

The conversion from $Dronpa^{D}$ and $Dronpa^{B}$ is primed at the excited states of the protonated and deprotonated states of the chromophore, respectively. The dark-to-bright conversion probably involves the excited-state proton transfer because the acidity of the hydroxyphenyl moiety is likely to be much higher in $S_1$ than $S_0$ (17, 18). By contrast, the bright-to-dark conversion is mysterious. How does the photoexcited chromophore protonate? An intriguing possibility is that the protonation follows an intersystem crossing to the first triplet state ($T_1$). It is generally accepted that the acidity of a phenol ring is lower in $T_1$ than in $S_1$ (19). The long lifetime of $T_1$ may also increase the probability of protonation. Interestingly, the presence of an intersystem crossing pathway after excitation of $Dronpa^{B}$ was predicted from a single-molecule analysis of Dronpa (20). Furthermore, the inefficient occurrence of an intersystem crossing may well account for the low quantum yield for the bright-to-dark conversion (0.00032) (4). Additional studies using phosphorescence spectroscopy will be required to understand the mechanism in greater detail. The dark-state electron density calculated from the deposited data appears consistent with a *trans* conformation for the chromophore, consistent with the interpretation provided by Andresen *et al.* (8). However, this model is one of several possible interpretations, because the electron density for the hydroxyphenyl group is not well resolved. Consequently, an alternate interpretation may be that multiple chromophore configurations coexist in the crystal, or that the phenolic end is substantially disordered in the dark state. In any case, protonation is the primary process in the bright-to-dark conversion. *cis-trans* isomerization may occur subsequently. In fact, a quantum chemical calculation predicts that the excited deprotonated chromophore has no driving force to rotate the $C^{\alpha}$-$C^{\beta}$ bond for isomerization (21).

The route of protonation of the chromophore may also be deduced from the crystallographic data of $Dronpa^{B}$. There is a crevice on the β-barrel arising from incomplete hydrogen bonding between strands 7 and 10 (Fig. 5*B*). Ile-195 is located on the rim of the crevice (Fig. 5 *B* and *C*). The amino group of Ile-195 may relay protons by interacting with the imidazole ring of His-194 outside and a water molecule (w46) inside the barrel. This water molecule (w46) directly interacts with the chromophore hydroxyl moiety at a distance of 2.78 Å and may regulate protonation. Based on crystallographic and spectroscopic data of *Aequorea* GFP variants, Agmon (22) has proposed proton pathways across the β-barrel wall. According to this model, chromophore excitation induces a conformational change opening the Thr-203 switch and expelling a proton. In the ground state, the chromophore is reprotonated by Glu-222, which in turn acquires a proton from the surrounding solvent via surface-bound glutamate residues. Thus, the Ile-195-mediated relay of protons that we have identified in Dronpa is unique. Furthermore, proton supply from the solvent is supported by the

**Table 1. Mutations crucial for monomerization and photochromism**

| Mutations | | | | | | Quaternary structure* | Conversion from $Dronpa^{B}$ to $Dronpa^{D}$† |
|---|---|---|---|---|---|---|---|
| 102 | 114 | 162 | 194 | 205 | 218 | | |
| I | F | L | R | N | G (22G) | 4 | – |
| I | F | L | R | N | **E** | 4 | ++ |
| **N** | F | L | R | N | G | 2–4 | – |
| **N** | F | L | R | N | **E** | 1 | ++ |
| **N** | **Y** | **S** | **H** | **S** | **E** (Dronpa) | 1 | +++ |

Boldface indicates the residues found in Dronpa.
*Determined by pseudonative electrophoresis (15).
†Determined by decreasing rate of absorbance at 503 nm upon continuous irradiation at 490 nm (4).

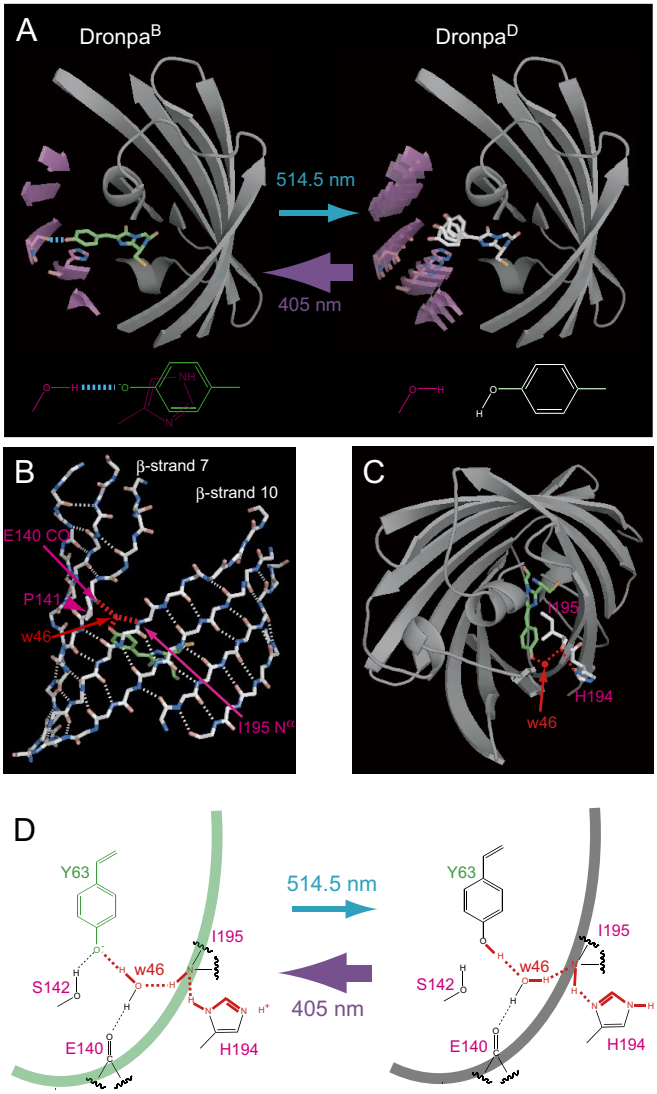


**Fig. 5.** A proposed mechanism for the Dronpa photochromism. (*A*) Schematic of structural flexibility of Dronpa induced by illumination at 514.5 and 405 nm. (*Left*) The deprotonated chromophore is tethered to and stacked by the β-barrel. The hydrogen bond between the chromophore and the Ser-142 hydroxyl group is indicated (dotted cyan line). (*Right*) The protonated chromophore is free from the β-barrel. As a result, the chromophore and a part of the β-barrel (purple) are flexible. (*B*) β-Strands 2, 3, 7, 8, 9, 10, and 11 of the Dronpa$^B$ crystal structure. Main chains with hydrogen bonds (dotted white lines) are shown. Pro-141 (magenta arrowhead) distorts β-strand 7 to form a crevice. w46 (red arrow) forms hydrogen bonds (dotted red line) with the chromophore hydroxyl moiety, the Ile-195 amino group (magenta arrow), and Glu-140 carbonyl group (magenta arrow). (*C*) Hydrogen-bond network (dotted red line) connecting the chromophore with His-194. (*D*) Light-induced rearrangement of the network (red line) that consists of hydrogen bonds (dotted line) and covalent bonds (solid line).

acid-sensitivity of Dronpa$^B$ (4). Although the glutamate residue corresponding to Glu-222 in *Aequorea* GFPs is conserved among all fluorescent proteins, the crystal structure of Dronpa$^B$ (5) does not reveal that the corresponding residue in Dronpa (Glu-211) supplies protons to the chromophore.

Here, we present a molecular mechanism for photochromism of a fluorescent protein. The mechanism requires a special microenvironment involving a β-barrel, a structure not present in organic photochromic compounds. In the photochromic fluorescent protein, Dronpa, light-induced protonation and deprotonation of the chromophore are intimately linked with changes in flexibility of the surrounding structure. The fluorescence of the protein is regulated by the degree of flexibility of the chromophore but is not necessarily accompanied by *cis-trans* isomerization. We note that the structurally characterized fluorescent proteins with high quantum yields have *cis*/coplanar chromophores, whereas those with low-fluorescence quantum yields have *trans*/noncoplanar chromophores (23–27). Accordingly, *cis-trans* isomerization of the chromophore in Dronpa has been considered an attractive mechanism for the photochromism of this protein (6, 8, 28). However, whereas structural rigidity is critical for high-fluorescence quantum yield, whether the two rings of the chromophore are in a *cis* or *trans* configuration is inconsequential. Notably, Henderson and Remington (29) proposed the importance of structural rigidity for fluorescence. Their study points out that the chromophore of a bright fluorescent protein, amFP486, is stabilized by His-199; a similar interaction between the chromophore and a histidine residue (His-193) is present in Dronpa$^B$. In addition, Henderson *et al.* (30) presented a comprehensive interpretation of the photochromism and *cis-trans* isomerization for a fluorescent protein mTFP0.7; they demonstrate that the *cis* isomer is highly ordered, whereas the *trans* isomer is nonplanar and disordered.

Dronpa$^B$ has a *cis*/coplanar chromophore in the rigid β-barrel. We demonstrate structural flexibility of the chromophore and a part of the β-barrel of Dronpa$^D$ with NMR analyses of both Dronpa$^B$ and Dronpa$^D$ in solution. Given the specific characteristics of photochromism in this protein, the critical flexibility within this structure may be difficult to identify by protein crystallography at extremely low temperatures.

## Methods

**Gene Construction.** For bacterial expression of Dronpa with a histidine tag at the N terminus, an NdeI-EcoRI fragment of Dronpa was inserted into the NdeI/EcoRI site of pET28a vector (Novagen) to generate the plasmid pET28a/Dronpa. For *in vitro* translation of Dronpa with a histidine tag at the C terminus, an NdeI-XhoI fragment of Dronpa including a C-terminal thrombin cleavage site was inserted into the NdeI-XhoI site of pIVEX2.3d vector (Roche) to generate the plasmid pIVEX2.3d/Dronpa.

**Protein Preparation.** For x-ray crystallography, proteins were expressed in *Escherichia coli* [JM109 (DE3)] transformed with pET28a/Dronpa or pRSET/22G (4) and purified as described (4). The histidine tag was removed by treatment with thrombin (Novagen) according to the manufacturer's instructions. A Ni-NTA agarose column (Qiagen) was then used to obtain Dronpa protein lacking the His-tag. The 22G was used without removing the tag. For NMR measurements, U-$^{13}C$,$^{15}N$-labeled Dronpa was prepared according to an established protocol (31). Briefly, *E. coli* strain BL21(DE3) (Invitrogen) transformed with pET28a/Dronpa was grown at room temperature in M9 media that contained U-$^{13}C$ glucose (2 mg/ml) and $^{15}NH_4Cl$ (1 mg/ml). Protein production was induced by addition of 10 mM isopropyl-β-D-thiogalactopyranoside. Purification, treatment with thrombin, and removal of the histidine tag were performed as described for x-ray crystallography samples. Specific labeling was carried out by using the RTS 500 ProteoMaster *E. coli* kit (Roche) using the amino acid mixture containing L-tyrosine-$^{13}C_9$,$^{15}N$ (Isotec) or L-histidine-$^{13}C_6$,$^{15}N_3$ (Isotec) in the presence of the RTS GroE supplement (Roche).

**X-Ray Crystallography.** Crystals were grown by the vapor-diffusion method in sitting-drop plates. Diffraction patterns were acquired by using a beamline BL44B2 or BL26B1 at SPring-8. Data were merged and processed by using the HKL2000 package (32). The structure was solved by the molecular replacement technique using the program Molrep (33). A protomer of the DsRed structure (PDB ID 1GGX) was used as a search probe. Crystallographic statistics are summarized in Table S1. The Dronpa crystal on the beamline was illuminated by an argon ion laser (514.5 nm, 150 mW; Melles Griot) and a laser diode (405 nm, 30 mW; Point Source) or a violet light (400DF15) from a 75-W xenon lamp. Fluorescence from the crystal was monitored by using a photonic multichannel analyzer PMA-11 (Hamamatsu Photonics). Structures are depicted with Mac PyMol (www.pymol.org) and TURBO-FRODO (Bio-Graphics).

**NMR Spectroscopy.** Proteins were reconstituted at a final concentration of 1 mM in 20 mM phosphate buffer (pH 7.5) containing 50 mM NaCl and 2% $D_2O$ (Isotec). Resonances were recorded in a Shigemi tube (Shigemi). All spectra except for one-dimensional $^1H$ spectra were acquired at 27°C by using a Bruker AVANCE 600-MHz spectrometer (Bruker BioSpin) equipped with a TCI cryoprobe (Bruker BioSpin). For recording of Dronpa$^D$, the sample was continuously illuminated by a 514.5-nm laser line from an argon ion laser (150 mW; Melles Griot) through a multimode optical fiber V50-MM (core diameter, 50 $\mu$m; Suruga Seiki,). Sequential resonance assignments for backbone $^1HN$, $^{13}C^{\alpha}$, $^{13}C^{\beta}$, and $^{15}N$ nuclei for Dronpa$^D$ and Dronpa$^B$ were derived from three-dimensional HNCACB and CBCACONH datasets of U-$^{13}C$,$^{15}N$-labeled Dronpa. NMR data were processed by using TopSpin (Bruker BioSpin) and CARA (www.nmr.ch). CSD was calculated as described (9).

**ACKNOWLEDGMENTS.** We thank H. Hosoi and A. Ohno for fruitful discussion and K. I. Tong, K. Otsuki, and M. Usui for technical assistance. This work was partly supported by grants from the Human Frontier Science Program, Molecular Ensemble Program at RIKEN, Japan MEXT Grant-in-Aid for Scientific Research on priority areas, Japan MEXT and Japan Society for the Promotion of Science for Grants-in-Aid for Scientific Research B, and Canadian Institutes for Health Research.

1. Dürr H, Bouas-Laurent H, eds *Photochromism* (Elsevier, Amsterdam), p 203.
2. Irie M (2000) Diarylethenes for memories and switches. *Chem Rev* 100:1685–1716.
3. Berkovic G, Krongauz V, Weiss V (2000) Spiropyrans and spirooxazines for memories and switches. *Chem Rev* 100:1741–1753.
4. Ando R, Mizuno H, Miyawaki A (2004) Regulated fast nucleocytoplasmic shuttling observed by reversible protein highlighting. *Science* 306:1370–1373.
5. Wilmann PG, *et al.* (2006) The 1.7 Å crystal structure of Dronpa: A photoswitchable green fluorescent protein. *J Mol Biol* 364:213–224.
6. Stiel AC, *et al.* (2007) Structural basis for reversible photoswitching in Dronpa. *Biochem J* 402:35–42.
7. Nam KH, *et al.* (2007) Structural characterization of the photoswitchable fluorescent protein Dronpa-C62S. *Biochem Biophys Res Commun* 354:962–967.
8. Andresen M, *et al.* (2007) Structural basis for reversible photoswitching in Dronpa. *Proc Natl Acad Sci USA* 104:13005–13009.
9. Mal TK, *et al.* (2004) Structural and functional characterization on the interaction of yeast TFIID subunit TAF1 with TATA-binding protein. *J Mol Biol* 339:681–693.
10. Tsien RY (1998) The green fluorescent protein. *Annu Rev Biochem* 67:509–544.
11. Bertini I, Felli IC, Kümmerle R, Moskau D, Pierattelli R (2004) $^{13}C$-$^{13}C$ NOESY: An attractive alternative for studying large macromolecules. *J Am Chem Soc* 126:464–465.
12. Egan W, Shindo H, Cohen JS (1978) On the tyrosine residues of ribonuclease A. *J Biol Chem* 253:16–17.
13. Wilbur DJ, Allerhand A (1976) Titration behavior of individual tyrosine residues of myoglobins from sperm whale, horse, and red kangaroo. *J Biol Chem* 251:5187–5194.
14. Tyukhtenko SI, *et al.* (2002) NMR studies of the hydrogen bonds involving the catalytic triad of *Escherichia coli* thioesterase/protease I. *FEBS Lett* 528:203–206.
15. Karasawa S, Araki T, Yamamoto-Hino M, Miyawaki A (2003) A green-emitting fluorescent protein from Galaxeidae coral and its monomeric version for use in fluorescence labeling. *J Biol Chem* 278:34167–34171.
16. Seifert MH, *et al.* (2003) Backbone dynamics of green fluorescent protein and the effect of histidine 148 substitution. *Biochemistry* 42:2500–2512.
17. Chattoraj M, King BA, Bublitz GU, Boxer SG (1996) Ultra-fast excited state dynamics in green fluorescent protein: Multiple states and proton transfer. *Proc Natl Acad Sci USA* 93:8362–8367.
18. Fron E, *et al.* (2007) Ultra-fast excited state dynamics in green fluorescent protein: Multiple states and proton transfer. *J Am Chem Soc* 129:4870–4871.
19. Turro NJ (1991) *Modern Molecular Photochemistry* (Univ Sci Books, Mill Valley, CA).
20. Habuchi S, *et al.* (2005) Reversible single-molecule photoswitching in the GFP-like fluorescent protein Dronpa. *Proc Natl Acad Sci USA* 102:9511–9516.
21. Weber W, Helms V, McCammon JA, Langhoff PW (1999) Shedding light on the dark and weakly fluorescent states of green fluorescent proteins. *Proc Natl Acad Sci USA* 96:6177–6182.
22. Agmon M (2005) Proton pathways in green fluorescent protein. *Biophys J* 88:2452–2461.
23. Prescott M, *et al.* (2003) The 2.2 Å crystal structure of a Pocilloporin pigment reveals a nonpolar chromophore conformation. *Structure (London)* 11:275–284.
24. Wilmann PG, Petersen J, Devenish RJ, Prescott M, Rossjohn J (2005) Variations on the GFP chromophore: A polypeptide fragmentation within the chromophore revealed in the 2.1-Å crystal structure of a nonfluorescent chromoprotein from *Anemonia sulcata*. *J Biol Chem* 280:2401–2404.
25. Quillin ML, *et al.* (2005) Kindling fluorescent protein from *Anemonia sulcata*: Dark-state structure at 1.38 Å resolution. *Biochemistry* 44:5774–5787.
26. Wilmann PG, *et al.* (2005) The 2.1 Å crystal structure of the far-red fluorescent protein HcRed: Inherent conformational flexibility of the chromophore. *J Mol Biol* 349:223–237.
27. Andresen M, *et al.* (2005) Structure and mechanism of the reversible photoswitch of a fluorescent protein. *Proc Natl Acad Sci USA* 102:13070–13074.
28. Lukyanov KA, Chudakov DM, Lukyanov S, Verkhusha VV (2005) Innovation: Photoactivatable fluorescent proteins. *Nat Rev Mol Cell Biol* 6:885–891.
29. Henderson JN, Remington SJ (2005) Crystal structures and mutational analysis of amFP486, a cyan fluorescent protein from *Anemonia majano*. *Proc Natl Acad Sci USA* 102:12712–12717.
30. Henderson JN, Ai HW, Campbell RE, Remington SJ (2007) Structural basis for reversible photobleaching of a green fluorescent protein homologue. *Proc Natl Acad Sci USA* 104:6672–6677.
31. Ikura M, *et al.* (1990) 3D NMR and isotopic labeling of calmodulin. Towards the complete assignment of the $^1H$ NMR spectrum. *Biochem Pharmacol* 40:153–160.
32. Otwinowski Z, Minor W (1997) Processing of x-ray diffraction data collected in oscillation mode. *Methods Enzymol* 276:307–326.
33. Collaborative Computational Project, Number 4 (1994) The CCP4 Suite: Programs for Protein Crystallography. *Acta Crystallogr D* 50:760–763.